Photophysics of excitons in quasi-one-dimensional organic semiconductors: Single-walled carbon nanotubes and π-conjugated polymers

H. Zhao and S. Mazumdar
Department of Physics, University of Arizona, Tucson, Arizona 85721, USA

C.-X. Sheng, M. Tong, and Z. V. Vardeny
Department of Physics, University of Utah, Salt Lake City, Utah 84112, USA
(Received 1 September 2005; revised manuscript received 21 November 2005; published 1 February 2006)

The nature of the primary photoexcitations in semiconducting single-walled carbon nanotubes (S-SWCNTs) is of strong current interest. We have studied the emission spectra of S-SWCNTs and two different π-conjugated polymers in solutions and films, and have also performed ultrafast pump-probe spectroscopy on these systems with unprecedented spectral range from 0.1 to 2.6 eV. The emission spectra relative to the absorption bands are very similar in S-SWCNTs and polymers, with redshifted photoluminescence in films showing exciton migration. We also found that the transient excited state spectra of both polymers and SWCNTs contain two prominent photoinduced absorption (PA) bands (PA_1 and PA_2) that are due to photogenerated excitons; in the polymers these PA bands are correlated with a stimulated emission band, which is absent in the S-SWCNTs. In order to understand the similarities in the PA spectra we have performed theoretical calculations of excited state absorptions in π-conjugated polymers as well as S-SWCNTs within the same correlated electron Hamiltonian. We find strong similarities in the excitonic energy spectra of these two classes of quasi-one-dimensional materials, although there exist also subtle differences such as the occurrence of dark excitons below the optical excitons in the S-SWCNTs. In the polymers PA_1 is an excited state absorption from the optical exciton to a two-photon exciton that occurs below the continuum band threshold. In the S-SWCNTs PA_1 occurs from both the optical exciton and the dark exciton, to final states which are close in energy and again below the continuum band threshold. PA_1 therefore gives the lower limit of the binding energy of the lowest optical exciton in both π-conjugated polymers and S-SWCNTs. The binding energy of lowest exciton that belongs to the widest S-SWCNTs with diameters $\geqslant 1$ nm in films is 0.3–0.4 eV, as determined by both experimental and theoretical methods.

DOI: 10.1103/PhysRevB.73.075403 PACS number(s): 78.47.+p, 71.35.Cc, 73.22.−f, 78.67.Ch

I. INTRODUCTION

Single-walled carbon nanotubes (SWCNTs) are of considerable current interest because of their unique mechanical,[1] electrical,[2] and optoelectronic[3,4] properties. Metallic (M-) versus semiconducting (S-) character of SWCNTs are determined by their diameters and chiralities, but in all cases extended dimensions along the tube axes and nanometer scale diameters render these systems quasi-one-dimensional (quasi-1D). Spatial separation of SWCNTs has recently become possible,[5] and this has led to intensive studies of the photophysics of S-SWCNTs. Different experiments have begun to indicate that primary photoexcitations in these systems are excitons, rather than free electrons and holes that are expected within one-electron theory.[6] Exciton formation in S-SWCNTs is a direct consequence of the combined effects of Coulomb electron-electron (e-e) interaction and the confinement that occurs in 1D. It is, for example, well known that confinement effects in 1D lead to unconditional exciton formation upon electron-hole (e-h) excitation, and excitons in nanowires of conventional semiconductors have been described within the 1D hydrogenic model, with deep excitons states and discrete energy spectrum below a Rydberg continuum.[7] Recent theories of linear optical absorptions in S-SWCNTs have emphasized the strong e-h interactions and the consequent exciton formation in these systems.[8–17]

In spite of the above theoretical and experimental investigations, the knowledge base about the physical nature of the optical excitons or the complete excitonic energy spectrum in S-SWCNTs remains incomplete. Whether or not the 1D hydrogenic model can be applied without modifications to S-SWCNTs is unclear, and there is also no consensus as yet on important materials parameters such as the exciton binding energy. One important reason for this is that the standard technique of comparing the thresholds of linear absorption and photoconductivity for the determination of the exciton binding energy fails in noncrystalline organic materials because of the existence of disorder and inhomogeneity in these systems. More recent experimental probes of S-SWCNTs have therefore focused on *nonlinear absorption*, which can give information on the nature of excited states occurring above the optical exciton. Several research groups have performed transient photomodulation (PM) experiments,[18–22] which have provided valuable information on the excitation dependence of photoluminescence (PL) and radiative versus nonradiative relaxation channels. A two-photon fluorescence measurement has given the first information on the lowest two-photon state that occurs above the lowest optical exciton in S-SWCNTs with diameters within a certain range.[23] Experimental results were interpreted within the context of the 1D hydrogenic model. In addition joint experiment-theory work on electroabsorption in S-SWCNTs has recently been performed.[24]

It is relevant in this context to recall that there exists already a vast literature on excitons in the π-conjugated polymer system, the *other* class of carbon-based quasi-1D systems. In order to seek guidance from this knowledge base, we have performed the same transient PM experiments with S-SWCNTs that were previously performed with the polymers.[25,26] We have also performed theoretical calculations of the excited state electronic structures and excited state absorptions for ten different S-SWCNTs with a wide range in diameters, within the same correlated electron model that has been widely applied to π-conjugated polymers.[27–35] We found strong similarities in the excitonic energy spectra of S-SWCNTs and π-conjugated polymers, in spite of the fact that carbon nanotubes are derived from two-dimensional (2D) graphitic layers and the coordination number per carbon atom is 3 instead of 2.

In the following sections we present the results of our experimental and theoretical investigations. We begin by pointing out the similarities in the linear optical absorption and fluorescence in S-SWCNTs and two different π-conjugated polymers. Following this, we present the results of our ultrafast pump-probe measurements on the same systems. Remarkable similarities between the S-SWCNTs and π-conjugated polymers are found. Finally, we present our theoretical work within the context of a correlated π-electron Hamiltonian. We briefly review the known results for the excitonic energy spectrum of π-conjugated polymers within the model Hamiltonian, and then proceed to discuss our results obtained for the S-SWCNTs. Our main message is that the photophysics of these two classes of materials is determined predominantly by their quasi-1D nature. Our results and conclusions also suggest possible directions for future optical investigations of S-SWCNTs.

II. EXPERIMENTAL SETUP

A. Sample preparation

In order to measure the ultrafast dynamic response of unbundled SWCNTs in the mid- to near-IR spectral range (0.1 to 1 eV), it was necessary to fabricate a transparent solid sample in the broadest spectrum possible that contains isolated nanotubes. To achieve this, 0.005% HiPCO-produced SWCNTs were mixed with 0.610% sodium dodecyl sulfate (SDS) surfactant and 0.865% polyvinyl alcohol (PVA) in deionized water. Sonication for an hour before sample preparation resulted in relatively well-separated nanotubes as made evident by the sharp features in the absorption spectrum [Fig. 1(b)]. We then deposited a film of the solution onto CaF_2 by drop-casting at 80 °C. The film consisted of mostly separated SWCNTs (with some bundling) embedded in an insulating matrix of PVA having an optical density of ~1 in the visible/near-IR spectral range (Fig. 1). Neither PVA nor SDS has absorption bands in the spectral range over which we measured the absorption and transient PM spectra. Resonant Raman scattering of the radial breathing mode was used to determine that the nanotubes in our sample have a diameter distribution around the mean diameter of ~0.8 nm, and contain about 1/3 metallic and 2/3 semiconducting SWCNTs.

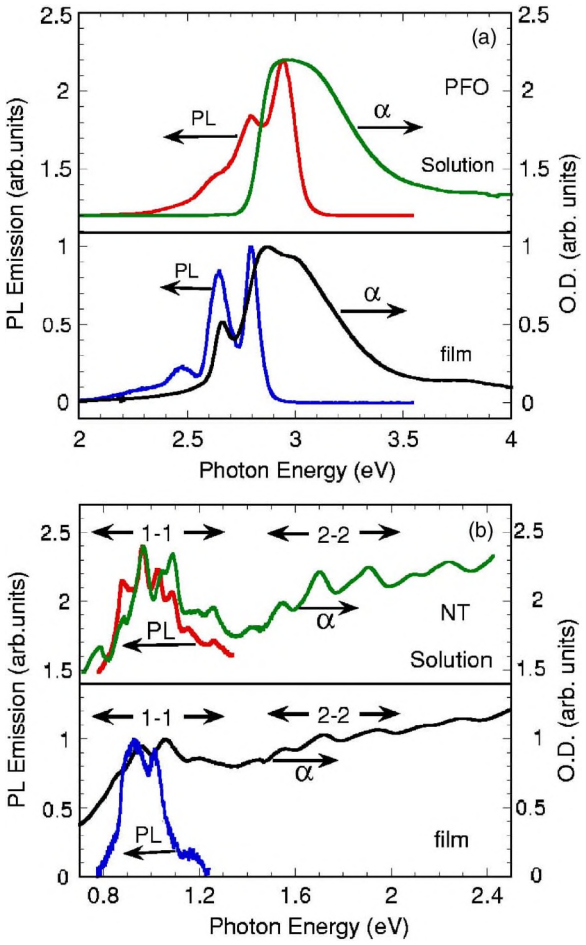

FIG. 1. (Color online) Photoluminescence (PL) emission and absorption $\alpha(\omega)$ spectra of (a) PFO solution and film, and (b) isolated SWCNTs in D_2O solution and PVA matrix film. The optical transitions 1-1 and 2-2 for SWCNT are assigned.

SWCNT samples in solution were prepared by dispersion of predominantly isolated nanotubes in D_2O, using a procedure based on the method developed by O'Connell *et al.*[5] The sonicated samples were first centrifuged for 10 min at 700 g. The upper 75% of the supernatant was recovered using a small-bore pipette, avoiding sediment at the bottom, and transferred to a Beckman centrifuge tube for further centrifugation. Samples were then centrifuged for 2 h at 4 °C. The upper 50% of the supernatant was then recovered using a small-bore pipette, avoiding sediment at the bottom, and transferred to a clean tube.

The semiconducting polymers used in our studies were a poly(para-phenylene vinylene) (PPV) derivative: dioctyloxy-PPV (DOO-PPV) that was synthesized in our laboratory using a published procedure,[36] and a blue poly(9,9-dioctylfluorene) (PFO) derivative that was purchased from American Dye Corp. (Canada) and used as is. Solutions were obtained by dissolving the polymer powder in toluene with concentration of ~1 mg/ml; films were obtained from the solution drop-casting onto CaF_2 substrates.

B. The optical setup

Our experimental studies involved mostly three kinds of measurements: transient PM, PL spectra, and absorption

spectra. For our transient PM measurements we used the fs two-color pump-probe correlation technique with linearly polarized light beams from two different experimental setups based on Ti:sapphire lasers, *with a broad spectral range from* 0.1 *to* 2.6 eV *and* 150 fs *time resolution*. To achieve such a broad spectral range we used two laser systems: a low power, high repetition rate laser with energy per pulse of ~0.1 nJ that was used for the mid-IR spectral range; and a high power low repetition rate laser with energy per pulse of ~10 μJ that was used in the near-IR to visible spectral range. The transient PM spectra from the two laser systems were normalized to each other at several probe wavelengths in the near-IR spectral range.

The ultrafast laser system used in the mid-IR spectral range for the low power measurements was a 100 fs Ti:sapphire oscillator (Tsunami, Spectra-Physics) which operated at a repetition rate of about 80 MHz, and pumped an optical parametric oscillator (Opal, Spectra-Physics). The Opal generates signal (S) and idler (I) beams that were used as probes with photon energy $\hbar\omega_S$ and $\hbar\omega_I$ ranging between 0.55 and 1.05 eV. In addition, these two beams were also mixed in a nonlinear crystal ($AgGaS_2$) to generate probe at $\omega_{\text{probe}}=\omega_S-\omega_I$ in the spectral range of 0.13 to 0.43 eV. The pump beam for SWCNTs was the fundamental at 1.6 eV; whereas for the polymers we used the second harmonic of the fundamental at 3.2 eV. The low energy per pulse produces low photoexcitation density of the order of 10^{16} cm^{-3}. With such low density we avoided the problem of exciton-exciton annihilation that could complicate the decay dynamics, or two-photon absorption (TPA) processes that may generate photoexcitations with very large excess energy. To increase the signal-to-noise ratio, an acousto-optical modulator operating at 85 kHz was used to modulate the pump beam intensity. In order to measure the transient response at time t with time resolution of ~150 fs, the probe pulses were mechanically delayed with respect to the pump pulses using a translation stage; the time $t=0$ was obtained by a cross-correlation between the pump and probe pulses in a nonlinear optical crystal. The pump and probe beams were carefully adjusted to get complete spatial overlap on the film, which was kept under dynamic vacuum. In addition, the pump/probe beam-walk with the translation stage was carefully monitored and the transient response was adjusted by the beam-walk measured response.

For the visible and near-IR measurements we used a homemade Ti:sapphire laser amplifier system that operated at ~1 kHz. The laser beam was split into two beams. The main part of the laser beam (~96%) was used as is for pumping the SWCNT samples, or frequency doubled in a nonlinear crystal to 3.2 eV for pumping the polymer samples. The other 4% of the amplifier output generated white light supercontinuum pulses in a glass substrate within the spectral range from 1.2 to 2.6 eV that was used as a probe. The pump and probe beams were carefully adjusted to get complete spatial overlap on the sample.

For measuring the PL spectra we used a standard continuous wave (cw) setup comprised of a pump laser (Ar^+ laser for the polymers and Ti:sapphire for the SWCNT samples), a $\frac{1}{4}$-meter monochromator and solid-state detectors (Si diode for the polymers and Ge diode for the SWCNT samples). A phase sensitive technique was used to enhance the signal-to-noise ratio. The absorption spectra were measured with commercially available spectrometers.

III. EXPERIMENTAL RESULTS

A. Linear absorption and fluorescence

We begin our comparison of the optical properties of π-conjugated polymers and S-SWCNTs with a discussion of the absorption $\alpha(\omega)$ and PL spectra of PFO and SWCNTs, in solutions and films (see Fig. 1). In all cases the spectra are inhomogeneously broadened. The lowest optical gap of S-SWCNTs is in the near-IR spectral range, whereas that of PFO is in the blue region of the visible spectral range. Within the one-electron tight-binding model[6] the 1-1 optical absorption band in SWCNTs is due to dipole allowed transitions from the highest valence subband to the lowest conduction subband, whereas the 2-2 transitions are from the next highest valence subband to the next lowest conduction subband, respectively. It is well known that the absorption bands of M-SWCNTs appear at $\hbar\omega > 1.6$ eV, and thus the S-SWCNTs in films are preferentially excited by the pump pulses at $\hbar\omega = 1.6$ eV. In contrast to the SWCNT films, $\alpha(\omega)$ of SWCNTs in D_2O solution [Fig. 1(b)] contains a number of distinct subbands. This shows that the inhomogeneity of the SWCNTs in D_2O solution is smaller than that in film. It is likely that in the solution the nanotubes are bundled together in specific groups with similar diameters, and thus exhibit more structured $\alpha(\omega)$ than in film.

In agreement with Kasha's rule,[37] which states that light emission occurs from the lowest energy level that is dipole-coupled to the ground state, PL emission bands in both PFO and SWCNT samples appear close to the low end of $\alpha(\omega)$. In the PFO solution spectra [Fig. 1(a)] the PL 1-1 band that occurs on the high energy side of the spectrum actually overlaps with the absorption band. The PFO film contains two phases of different polymer order (α and γ), where γ shows PL at lower energies.[38] The PL bands of both phases are redshifted relative to their respective absorption bands. As in the PFO solution, in the SWCNT solution spectrum [Fig. 1(b)] the PL bands also overlap with their respective 1-1 absorption bands. In the SWCNT film, in contrast, the PL bands are again redshifted with respect to their corresponding absorption bands, *exactly as in the PFO film*. The underlying mechanism of the redshifted PL band in PFO films was identified as exciton migration to the lowest energy sites.[39] Based on the redshifted PL emission in the SWCNT film, we therefore speculate that here too there occur *excitons* that migrate to the lowest energy "emission sites." The ease of exciton migration in both materials shows that the excitons are robust, with binding energies substantially larger than the binding energies of the shallow traps in the sample.

B. Ultrafast spectroscopy measurements

In Fig. 2 we compare the transient PM spectra of films of S-SWCNTs and two polymers at time $t=0$. The transient PM signal $\Delta T/T(t)$ is the fractional change in transmission T, and is negative for photoinduced absorption (PA), positive

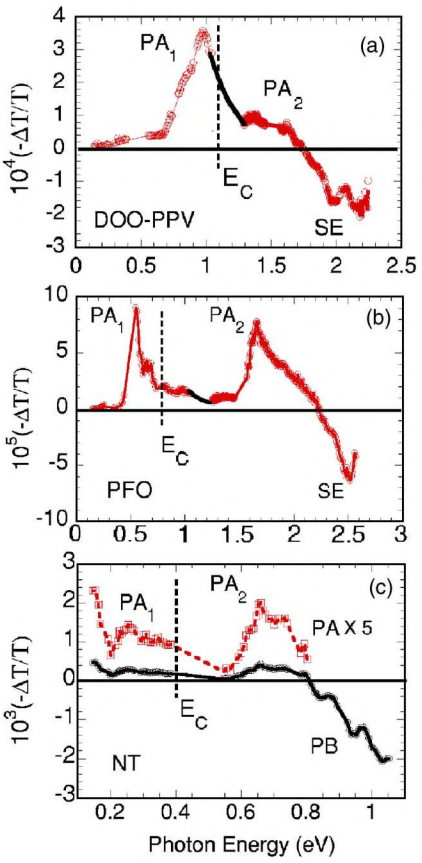

FIG. 2. (Color online) Transient PM spectra at $t=0$ of films of DOO-PPV (a), PFO (b), and isolated SWCNT in PVA matrix (c). Various PA, PB, and SE bands are assigned. The vertical dashed lines at E_c between PA_1 and PA_2 denote the estimated continuum band onset (see text).

for photoinduced bleaching (PB) and stimulated emission (SE). In none of the samples do we obtain a PA spectrum that increases at low energy in the shape of free carrier absorption, viz., $\Delta\alpha \sim \omega^{-2}$. Instead, the PA spectra are in the form of distinct photoinduced bands PA_1 and PA_2 associated with specific optical transitions of the primary photoexcitations in the samples, *which are therefore not free carriers*. The sharp PA rise below 0.2 eV in Fig. 2(c) is likely due to photogenerated "free" carrier absorption in M-SWCNTs. The free carriers may have been separated in the M-SWCNTs that are bundled together with S-SWCNTs following the original exciton photogeneration, and their consequent diffusion among various S-SWCNTs in the sample.

The PA and their respective PB (or SE) bands in both polymers and S-SWCNTs are correlated to each other (see Fig. 3). The lack of SE in the S-SWCNT PM spectrum shows that whereas excitons in polymers are radiative, excitons in the S-SWCNTs are not. The dominance of nonradiative over radiative recombination in S-SWCNTs has been ascribed to a variety of effects, including (a) trapping of the excitation at defect sites,[40] (b) strong electron-phonon coupling,[41] and (c) the occurrence of optically dark excitons below the allowed excitons.[15] Furthermore, from the correlated dynamics of the transient PB and PA bands we have previously concluded that PA originates from excitons in the $n=1$ manifold.[19,21]

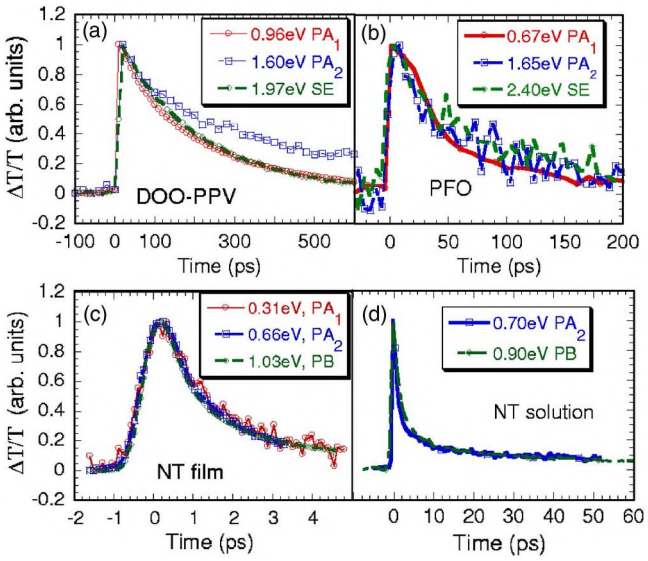

FIG. 3. (Color online) Transient PM dynamics at various probe energies in (a) DOO-PPV, (b) PFO, (c) SWCNT in PVA matrix, and (d) SWCNTs in D_2O solution.

Figure 3 summarizes the decay dynamics of the various bands in the PM spectra of these semiconductors. For each material the PA, PB, or SE bands have very similar dynamics and therefore they share a common origin, namely, the same primary excitation, which is the photogenerated exciton. In the case of polymer films [Figs. 3(a) and 3(b)] PA_1, PA_2, and SE decays are nonexponential, with the decay in DOO-PPV longer than that in PFO. It has been empirically determined that the decay time constant τ in the π-conjugated polymers is related to the PL quantum efficiency (QE) η by the relation[21,42]

$$\eta = \tau/\tau_{\mathrm{rad}}, \tag{1}$$

where τ_{rad} is the radiative lifetime of the 1D exciton, which is 1 ns in polymers.[25,26] From the ps exciton dynamics in Fig. 3 we estimate the decay time constants for polymers $\tau_{\mathrm{PPV}}=250$ ps [Fig. 3(a)], $\tau_{\mathrm{PFO}}=100$ ps [Fig. 3(b)], and get from Eq. (1) $\eta=25\%$ for DOO-PPV and $\eta=10\%$ for PFO; both η's are in excellent agreement with the PL QE that we measured using an integrated sphere.

Figures 3(c) and 3(d) show the decay dynamics of the photogenerated exciton in the S-SWCNT thin film and solution, respectively. The decay in the S-SWCNT film ($\sim$2 ps) [Fig. 3(c)] is much faster than that in the polymer film as well as that in the SWCNT solution. The likely origin of this is the bundling of the SWCNTs in the film, and exciton migration from S-SWCNTs to M-SWCNTs, the energy relaxation in which is relatively fast and nonradiative. The exciton decay in S-SWCNTs in solution [Fig. 3(d)] reflects isolated nanotube behavior and is composed of a fast and a slow component, similar to the recently measured PL(t) decay.[43] The correlation of transient PM and PL again shows that the PA is due to excitons in this material. We determined that the slow component PA lasts about 0.5 ns. From Eq. (1) for the QE of 1D excitons, and assuming that τ_{rad} for S-SWCNTs is the same as for π-conjugated polymers, viz.,

1 ns, we calculate $\eta \simeq 50\%$ for S-SWCNTs. The PL QE in S-SWCNTs in solution was, however, measured with an integrated sphere to be $\eta \approx 6 \times 10^{-4}$, and this shows that the radiative lifetime τ_{rad} for excitons in S-SWCNTs is very different than that in polymers. Actually from the measured η and the decay time constant of the slow PA component we calculate using Eq. (1) the radiative lifetime for S-SWCNTs $\tau_{rad} \approx 1$ μs, indicating that the bulk of the $n=1$ excitons that contribute to PA are nonradiative. The relative occupations of the dark and allowed exciton states, however, may depend very sensitively on extrinsic parameters such as temperature, pressure, electric and magnetic fields, etc. This seems to support the previous suggestion that rapid decay occurs in S-SWCNTs from the optical to the dark exciton with lower energy.[15] More recent theoretical work has also emphasized the influence of the dark exciton on the radiative recombination rates in SWCNTs.[44,45]

IV. π-ELECTRON EXCITON THEORY AND PHOTOPHYSICS

A. Theoretical model

The striking similarities in the transient PM spectra and in the cw PL with respect to absorption spectra $\alpha(\omega)$ of the polymeric semiconductors and the SWCNTs strongly suggest that the two families of materials should be described within the same fundamental theory. Common to both SWCNTs and semiconducting polymers are π-electrons, and we anticipate that the optical behavior is determined predominantly by these electrons. Whereas π-electron-only models miss the curvature effects associated with the narrowest SWCNTs, the low peak energy of the PA_1 band in Fig. 2(c) indicates that the photophysics of the S-SWCNTs in our sample is dominated by the widest SWCNTs (see below). We will thus be interested in generic consequences of *e-e* interactions that are valid for the widest S-SWCNTs. We therefore focus on the semiempirical Pariser-Parr-Pople (PPP) model Hamiltonian,[46,47] which has been widely applied to π-conjugated systems in the past,

$$H = -\sum_{\langle ij\rangle,\sigma} t_{ij}(c_{i\sigma}^{\dagger}c_{j\sigma} + c_{j\sigma}^{\dagger}c_{i\sigma}) + U\sum_{i} n_{i\uparrow}n_{i\downarrow} + \frac{1}{2}\sum_{i\neq j} V_{ij}(n_i - 1) \times (n_j - 1). \quad (2)$$

Here $c_{i\sigma}^{\dagger}$ ($c_{i\sigma}$) creates (annihilates) a π-electron on carbon atom i with spin σ ($\uparrow$, $\downarrow$), $\langle ij\rangle$ implies nearest neighbor (n.n.) sites i and j, $n_{i\sigma}=c_{i\sigma}^{\dagger}c_{i\sigma}$ is the number of electrons with spin σ on site i, and $n_i=\Sigma_\sigma n_{i\sigma}$ is the total number of electrons on site i. The parameter t_{ij} is the hopping integral between p_z orbitals of n.n. carbon atoms, U is the on-site Coulomb repulsion between two electrons occupying the same carbon atom p_z orbital, and V_{ij} is the long range intersite Coulomb interaction. In the case of the π-conjugated polymers t_{ij} are different for phenyl, single, and double carbon bonds. For the SWCNTs, however, they are the same (ignoring curvature effects). Longer range t_{ij} beyond n.n. can be included in Eq. (2), but previous experience indicates that these terms have only quantitative effects and do not give additional insight.

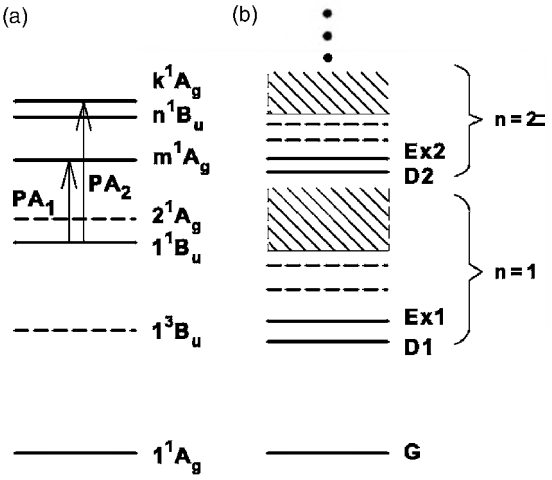

FIG. 4. Schematics of the excitonic electronic structures of (a) a light-emissive π-conjugated polymer and (b) a S-SWCNT. In (a) the lowest triplet exciton $1\,^3B_u$ occurs below the lowest singlet exciton $1\,^1B_u$. The lowest two-photon state $2\,^1A_g$ is composed of two triplets and plays a weak role in nonlinear absorption. Transient PA is from the $1\,^1B_u$ to the $m\,^1A_g$ two-photon exciton which occurs below the continuum band threshold state $n\,^1B_u$, and to a high energy $k\,^1A_g$ state that occurs deep inside the continuum band. In (b), $n=1$ and $n=2$ energy manifolds for S-SWCNT are shown. *Exn* and *Dn* are dipole-allowed and forbidden excitons, respectively. Shaded area indicate continuum band for each manifold. (Note that exciton levels of the $n=2$ manifold should be buried in the $n=1$ continuum band, but for clarity, the $n=1$ continuum band ends below *D*2.)

In contrast to the semiempirical approach used here, *ab initio* techniques have also been employed to theoretically investigate the exciton behavior of S-SWCNTs.[12–14] To date, however, the *ab initio* approach has been used to study linear absorption only. On the other hand, the photophysics and nonlinear absorptions of π-conjugated polymers have been widely investigated within the semiempirical Hamiltonian of Eq. (2),[27–35] and very recently a theory of linear absorption in S-SWCNTs was also advanced within this model.[15] For the sake of completeness, it is useful to first briefly discuss the theory of linear and nonlinear absorptions in π-conjugated polymers within the PPP model.

B. Excitons and excited state energy spectra of π-conjugated polymers

Unsubstituted π-conjugated polymers usually possess inversion symmetry, and thus their eigenstates are classified as either even parity A_g or odd parity B_u. Figure 4(a) shows schematically the theoretical excitation spectra of a light emissive π-conjugated polymer such as PFO or PPV.[32] Optical transitions corresponding to PA_1 and PA_2 are indicated as vertical arrows in the figure. The spin singlet ground state is $1\,^1A_g$. The lowest optical state $1\,^1B_u$ is an exciton. Although eigenstates within Eq. (2) are correlated, the $1\,^1B_u$ is *predominantly* a one electron-one hole ($1e$-$1h$) excitation relative to the correlated ground state.[48] The lowest two-photon state, the $2\,^1A_g$, is highly correlated and has strong contributions from triplet-triplet two electron-two hole

($2e$-$2h$) excitations.[29,33,35,48] There can occur other low energy $2e$-$2h$ triplet-triplet two-photon states above the $2\ ^1A_g$, but all such two-photon states participate weakly in PA or TPA,[27,48] because of their weak dipole couplings to the $1e$-$1h$ $1\ ^1B_u$. A different higher energy two-photon state [see Fig. 4(a)], referred to as the $m\ ^1A_g$ (where m is an unknown quantum number), has an unusually large dipole coupling with the $1\ ^1B_u$ and has been shown theoretically to dominate nonlinear absorption measurements.[27–29,35,48] The $m\ ^1A_g$ is the lowest predominantly $1e$-$1h$ two-photon exciton, and is characterized by greater e-h separation[48] than the $1\ ^1B_u$. The lower threshold state of the continuum band in Fig. 4(a) is referred to as the $n\ ^1B_u$.[28,35,48] Although there exist many other excited states in the infinite polymer, theory predicts that the $1\ ^1A_g$, $1\ ^1B_u$, $m\ ^1A_g$, and $n\ ^1B_u$ are the four *essential states*[27–33,35] that dominate the optical nonlinearity because of the very large dipole couplings among them.

Based on direct computations,[32] PA_1 in PPV and PFO corresponds to excited state absorption from the $1\ ^1B_u$ optical exciton to the $m\ ^1A_g$ two-photon exciton within the correlated electron picture. The $m\ ^1A_g$ exciton has been experimentally observed in PA,[25,26] TPA,[49] and electroabsorption.[28,50] Notice that Fig. 4(a) indicates that PA_1 gives the lower limit of the exciton binding energy. Given the widths of the experimental PA_1 bands in Figs. 2(a) and 2(b), and the theoretical uncertainty in the energy difference between the continuum band threshold and the $m\ ^1A_g$, we believe that the exciton binding energy is 0.8 ± 0.2 eV for PPV-DOO and 0.6 ± 0.2 eV for PFO.

PA_2 in π-conjugated polymers is to a distinct $k\ ^1A_g$ state that occurs deep inside the continuum band. Theoretical description of this state has been given by Shukla *et al.*[51] Specifically, in polymers with multiple bands within one-electron theory, there occur multiple classes of $2e$-$2h$ excited configurations, involving different bands. The exact $m\ ^1A_g$ and $k\ ^1A_g$ are both superpositions of $1e$-$1h$ and $2e$-$2h$ excitations, but the nature of the $2e$-$2h$ excitations that contribute to these states are different.

C. Computational procedure and parametrization for the S-SWCNTs

The results shown schematically in Fig. 4(a) have been obtained by solving the Hamiltonian of Eq. (2) using a variety of sophisticated many-body techniques, including exact diagonalization (full configuration-interaction, FCI) of small clusters[27–29] and the multiple reference single and double CI (MRSDCI).[51] The difficulty of these many-body calculations increases rapidly with system size, and they cannot be used for long oligomers of systems with large unit cells (such as PPV or PFO), and calculations of S-SWCNTs are simply out of question. Specifically for the investigation of polymers with large unit cells the essential states mechanism of optical nonlinearity has been reexamined within a diagrammatic exciton basis, which yielded pictorial descriptions of all excited states.[48] This approach showed that even within correlated-electron Hamiltonian the complete set of nonlinear optical channels can be classified into independent and separate subsets that involved dressed $1e$-$1h$ excitations, dressed $2e$-$2h$ excitations, etc. (see Fig. 12 in Ref. 48). Furthermore, the essential excitations $1\ ^1B_u$, $m\ ^1A_g$, and $n\ ^1B_u$ are *predominantly* $1e$-$1h$ (see Fig. 8 in Ref. 48). This suggests that with suitable parametrization of the Coulomb parameters that takes into account the dressing of the quasiparticles it should be possible to describe the $1\ ^1B_u$, $m\ ^1A_g$, and $n\ ^1B_u$ semiquantitatively in the space of single excitations from the Hartree-Fock (H-F) ground state. Reference 48 therefore provides the justification for using the single configuration-interaction (SCI) approximation,[30,32] which retains only the configuration mixing between $1e$-$1h$ excitations from the H-F ground state, to describe the energy range between the exciton and the continuum band in π-conjugated polymers. We have recently used the SCI approximation for calculating linear optical absorptions for S-SWCNTs.[15]

The SCI procedure we use follows the original formulation of Pople.[52] The initial step involves calculation of charge densities and bond orders from the eigenfunctions of the Hückel Hamiltonian [$U=V_{ij}=0$ limit of Eq. (2)] within the π-electron basis, which are then used as the inputs for the H-F matrix elements [see Eqs. (2.5) and (2.6) in Ref. 52]. The H-F ground state is obtained within the π-electron basis self-consistently. The SCI procedure now consists of calculating matrix elements of the interaction terms of PPP Hamiltonian between single excitations $\chi_{i\to j}$ and $\chi_{k\to l}$ from the H-F ground state (here $\chi_{i\to j}$ is a many-electron configuration in which an electron has been promoted from the bonding molecular orbital i to the antibonding molecular orbital j) using the expressions in the original Ref. 52 [see Eqs. (2.11) and (2.14) here], and diagonalizing the Hamiltonian matrix.

Actual implementation in our case also requires choosing the proper boundary conditions and determination of the right parameters that will describe the essential excitations at least semiquantitatively. Calculations of linear and nonlinear absorption require evaluations of the matrix elements of the transition dipole operator, which is not well defined[53] for periodic boundary condition (PBC) within Eq. (2). Instead of using approximate expressions for the dipole operator we have used the open boundary condition (OBC). For PPV this required calculations of oligomers with terminal phenyl groups. Optical absorption spectra calculated this way are qualitatively similar for oligomers of length greater than 4 unit cells and quantitatively identical for oligomers of length greater than 12 unit cells.[32] For the S-SWCNTs, there occur dangling bonds at the ends of the tubes, and hence surface states within the H-F band structure.[15] The surface states are easily detected from their size-independent midgap energies within the band structure, as well as from their wave functions. They are removed following the H-F calculations, prior to the evaluation of the SCI matrix elements. The overall SCI calculations quickly become prohibitively time consuming for long S-SWCNTs with large diameters. Hence the bulk of the calculations we report are for 20 unit cells for the zigzag S-SWCNTs and 10 unit cells for the chiral ones. We performed two different tests for each S-SWCNT to confirm that convergences in all energies have been reached to within 0.1 eV. First, in all cases we have ascertained that at the above tube lengths the tight-binding $U=V_{ij}=0$ optical gaps are identical within PBC and OBC, provided the surface state energies obtained with OBC are ignored. Second, for

each S-SWCNT the SCI calculations were performed for a series of lengths up to the maximum one. In all cases it was found that the energies of the two lowest S-SWCNT excitons and the lower threshold energies of the respective continuum bands had converged to within 0.1 eV. In addition to the above tests which were carried out for all S-SWCNTs for which we report results, for the two representative cases of the (11,0) zigzag S-SWCNT and the (6,2) chiral S-SWCNT, we performed an additional convergence test by performing SCI calculations for 40 and 20 unit cells, viz., twice the standard lengths, respectively. Detailed comparisons of various quantities for these representative cases are shown in the next section. From these comparisons, it should be obvious that the errors due to the OBC and finite sizes in the calculated exciton and continuum band threshold energies are less than 0.1 eV, thus validating our approach. The apparently faster convergence with the chiral S-SWCNTS (in terms of the number of unit cells) is due to the much larger number of carbon atoms in their unit cells.

We now come to the issue of parameters. We have performed our calculations with $t_{ij}=t=2.4$ eV, which is the most commonly used value for the hopping integral within correlated-electron models for π-conjugated systems.[54] Our parametrization of the V_{ij} was similar to the standard Ohno parametrization[55]

$$V_{ij}=\frac{U}{\kappa\sqrt{1+0.6117R_{ij}^2}}, \tag{3}$$

where R_{ij} is the distance between sites i and j in Å, and κ is a measure of the dielectric screening due to the medium.[32] In Ref. 32 we had done SCI calculations of the linear optical absorption in PPV with five different values of U (between 2 and 10 eV) and three different values of κ (1, 2, and 3) and had shown that only with $U=8$ eV and $\kappa=2$ was it possible to fit all four absorption bands in PPV (at 2.4, 3.7, 4.7, and 6 eV) quantitatively. In particular, the bare Ohno parameters ($U=11.26$ eV, $\kappa=1$) gave qualitatively incorrect results. Following the fitting of linear absorption, we also showed that with the same parameters it was possible to quantitatively fit nonlinear absorption measurements (see Fig. 6). Importantly, the correct energy of the lowest triplet exciton[56] was actually predicted in Ref. 32. Our choice of $U=8$ eV and $\kappa=2$ as the generic parameters for π-conjugated systems has been corroborated by more recent full CI studies of the energy spectra of several phenyl-based molecules,[57] for which experimental data for very high energy states can be found in the literature. We arrived at the same conclusion from our recent theoretical work on the linear absorption in the S-SWCNTs.[15] Predicted exciton binding energies with $U=8$ eV and $\kappa=2$ in this work for wide S-SWCNTs with diameters of 0.8 nm and greater seem to closely match subsequently determined experimental binding energies. Based on all these, we have chosen $U=8$ eV and $\kappa=2$ in our calculations of nonlinear absorptions in S-SWCNTs.

D. Linear absorption and one-photon excitons in S-SWCNTs

We have recently calculated the linear absorptions of ten different S-SWCNTs with diameters (d) ranging from 0.55 to 1.35 nm within the PPP model of Eq. (2), using the SCI approximation.[15] The list includes seven zigzag semiconductors between the (7,0) and the (17,0) SWCNTs (inclusive), and the (6,2), (6,4), and (7,6) chiral SWCNTs. In Fig. 4(b) we show schematically a summary of our calculations.[15] There occur multiple energy manifolds $n=1,2,\ldots$, etc., within the total energy scheme. Within each n, there occur optically dark excitons Dn a few k_BT below the optically allowed exciton Exn. In addition to the two nondegenerate excitons shown in Fig. 4(b) there also occur doubly degenerate dark excitons above Dn (see Table I in Ref. 15). These have not been included in Fig. 4(b) as they play no role in the photophysics (they are not optically connected to ground state, while the final exciton state reached in the relaxation from Exn must be the lowest energy Dn by Kasha's rule). Each manifold n has also its own H-F band gap that corresponds to the lower threshold of the continuum band within SCI theory. The binding energies of the excitons are then defined as the energy difference between the H-F band gaps and the excitons within the same manifold. We found that the binding energies of the $n=1$ and $n=2$ excitons decrease with increasing diameters, and they are nearly equal in the wide S-SWCNT limit. Our calculated binding energies for S-SWCNTs were in all cases smaller than those calculated for PPV or PFO using the same parameters. For the widest S-SWCNTs ($d\approx 1.3$ nm), our calculated exciton binding energies are close to 0.3 eV.

TABLE I. Calculated exciton energies E_{Exn}, exciton binding energies E_{bn}, $n=1,2$ and the energy difference δE between $Ex1$ and $D1$ for the (11,0) and (6,2) S-SWCNTs with OBC, for different nanotube lengths. All energies are in eV.

NT	No. of unit cells	No. of C atoms	E_{Ex1}	E_{b1}	δE	E_{Ex2}	E_{b2}
(11,0)	10	440	1.49	0.43	0.16	2.53	0.43
	20	880	1.31	0.41	0.08	2.19	0.45
	40	1760	1.26	0.41	0.05	2.12	0.45
(6,2)	6	624	1.81	0.53	0.09	3.22	0.73
	10	1040	1.77	0.53	0.06	3.22	0.72
	20	2080	1.76	0.52	0.04	3.30	0.63

As mentioned above, our calculations for the zigzag and chiral S-SWCNTs were for 20 and 10 unit cells, respectively. In Table I we compare the calculated exciton energies $Ex1$ and $Ex2$, their respective binding energies, and the energy difference δE between $Ex1$ and $D1$ for 10, 20, and 40 unit cells of the (11,0) S-SWCNT. The exciton binding energies are obtained by subtracting the exciton energies from the H-F bandgaps. From every perspective, it is clear that while at 10 unit cells finite size effects are still strong, at 20 unit cells the exciton energies and their binding energies have converged. Table I also lists the same quantities for 6, 10, and 20 units of the chiral (6,2) S-SWCNT, and now convergence is reached at 10 unit cells, for the reason already given above. The percentage error in δE at 20 and 10 unit cells of the zigzag and chiral nanotubes is relatively large, because of its small magnitude. This quantity, however, does not enter into our discussion of nonlinear absorption of S-SWCNTs.

Interestingly, our calculated E_{Ex1} for the (11,0) S-SWCNT at 40 unit cells (1.26 eV) is remarkably close to that calculated within the *ab initio* technique (1.21 eV)[45] although our δE (0.045 eV) is considerably larger than the *ab initio* value (0.029 eV). More detailed comparisons between the semiempirical and *ab initio* approaches will have to wait until more results for wide S-SWCNTs, including their exciton binding energies, become available within the *ab initio* approach.

E. Nonlinear absorption in S-SWCNTs

In the present work we performed SCI calculations of excited state absorptions using the parameters of Eq. (3), for all the S-SWCNTs in Ref. 15. The zigzag S-SWCNT calculations are for 20 unit cells, whereas the chiral S-SWCNT calculations are for 10 unit cells. Zigzag S-SWCNTs possess inversion symmetry, and therefore nondegenerate eigenstates are once again classified as A_g or B_u. Lack of inversion symmetry in chiral S-SWCNTs implies that their eigenstates are not strictly one-or two-photon states. Nevertheless, from explicit calculations of matrix elements of the dipole operator, we have found that eigenstates of chiral S-SWCNTs are *predominantly* one-photon (with negligible two-photon cross section) or *predominantly* two-photon states (with very weak one-photon dipole coupling to the ground state). We shall therefore refer to eigenstates of chiral S-SWCNTs as "A_g" and "B_u," respectively.

The nature of the ultrafast PA discussed in the previous section demonstrates that PA is due to excited state absorption from the $n=1$ exciton states. From Fig. 4(b), the excited state absorption can be from $Ex1$, as well as from $D1$, following rapid nonradiative decay of $Ex1$ to $D1$. As in the case of π-conjugated polymers,[48] we have evaluated all transition dipole couplings between the $n=1$ exciton states ($Ex1$ and $D1$) and all higher energy excitations. The overall results for S-SWCNTs are very similar to those in the π-conjugated polymers.

Our computational results are the same for all zigzag nanotubes. These are modified somewhat for the chiral nanotubes (see below), but the behavior of all chiral S-SWCNTs are again similar. In Figs. 5(a) and 5(b) we show the representative results for the zigzag (10,0) and the chiral (6,2) S-SWCNTs, respectively. The solid vertical lines in Fig. 5(a) indicate the magnitudes of the normalized dipole couplings between $Ex1$ in the (10,0) NT with all higher energy excitations e_j, $\langle Ex1|\mu|e_j\rangle/\langle Ex1|\mu|G\rangle$, where G is the ground state. The dotted vertical lines are the normalized transition dipole moments between the dark exciton $D1$ and the higher excited states, $\langle D1|\mu|e_j\rangle/\langle Ex1|\mu|G\rangle$. Both couplings are shown against the quantum numbers j of the final state along the lower horizontal axis, while the energies of the states j are indicated on the upper horizontal axis. The reason why only two vertical lines appear in Fig. 5(a) is that all other normalized dipole couplings are *invisible on the scale of the figure*. A striking aspect of the results for the (10,0) zigzag S-SWCNT are then that *exactly as in the π-conjugated polymers, the optical exciton $Ex1$ is strongly dipole-coupled to a single higher energy $m\,^1A_g$ state*. The dark exciton $D1$ is similarly strongly coupled to a single higher energy state (hereafter the $m'\,^1A_g$). Furthermore, the dipole couplings between $Ex1$ and $m\,^1A_g$ (or $D1$ and $m'\,^1A_g$) are stronger than those between the ground state and the excitons, which is also true for the π-conjugated polymers.[48]

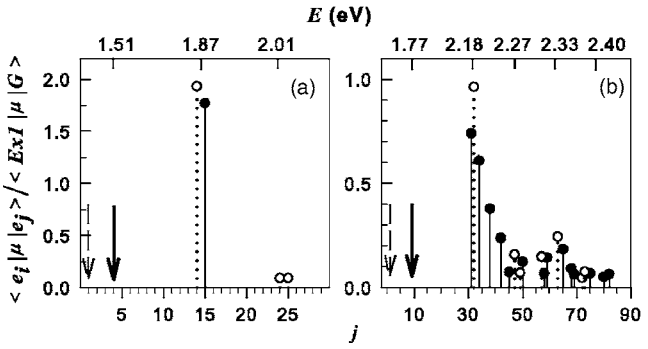

FIG. 5. Normalized transition dipole moments between S-SWCNT exciton states $Ex1$ and $D1$ and all other excited states e_j, where j is the quantum number of the state in the total space of single excitations from the H-F ground state. The numbers along the upper horizontal axes are energies in eV. Results shown are for (a) the (10,0), and (b) the (6,2) S-SWCNTs, respectively. Solid (dotted) lines correspond to $e_i=Ex1$ ($D1$). The solid and dashed arrows denote the quantum numbers of $Ex1$ and $D1$, respectively.

The situation in the chiral (6,2) S-SWCNT is slightly different, as shown in Fig. 5(b). Both the $Ex1$ and $D1$ excitons are now strongly dipole-coupled to several close-lying excited states, which form narrow "bands" of m'"^1A_g" and m'"$A_g{}^1$" states. Similar to the case of zigzag S-SWCNTs, these bands occur above the $Ex1$.

From the calculated results of Fig. 5 a simple interpretation to PA_1 in Fig. 2 emerges, viz., PA_1 is a superposition of excited state absorptions from $Ex1$ and $D1$. This raises the question whether PA_2 in the S-SWCNTs can be higher energy intersubband absorptions from the $n=1$ excitons to two-photon states that lie in the $n=2$ (or even $n=3$) manifolds. We have eliminated this possibility from explicit calculations: the transition dipole matrix elements between one-photon states in the $n=1$ manifold and two-photon states within the higher n manifolds are zero. As in the π-conjugated polymers, two-photon states giving rise to PA_2 cannot therefore be computationally accessed without taking into account the $2e$-$2h$ excitations[51] and are outside the scope of the present work.

In Fig. 6 we show the energy locations of all the relevant one- and two-photon states within the $n=1$ manifold for the (10,0) and (6,2) NTs. The figure includes the absolute energies of the Exn and Dn excitons, the two-photon $m\,^1A_g$ states and the corresponding H-F bandgaps for the (10,0) and (6,2) S-SWCNTs. The absolute energies depend strongly on the value of t_{ij} chosen in our calculations, and is slightly too high for the S-SWCNTs, as we have chosen the same $t_{ij}=2.4$ eV for the S-SWCNTs and the phenyl bonds in the π-conjugated polymers. We have found that with smaller t_{ij} (~1.8 eV), which take into account the curvature of the S-SWCNTs, the calculated absolute energies of the optical excitons are very close to the experimental values.[58] The differences between the energies of the eigenstates (for example, the binding en-

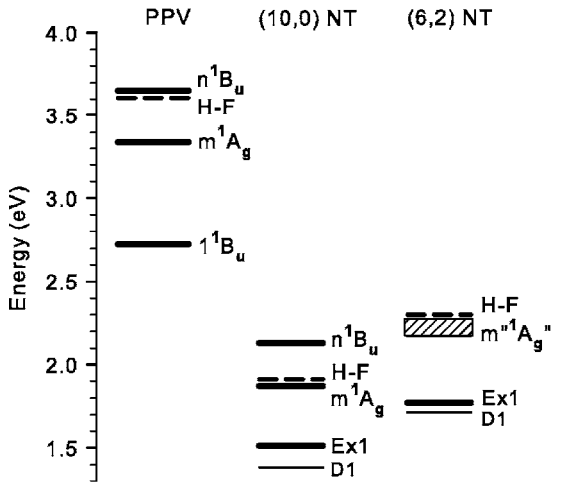

FIG. 6. SCI energies of optically relevant states in (from left to right) PPV, (10,0) SWCNT and (6,2) SWCNT, respectively. In all cases the $m\,^1A_g$ ($m"\,^1A_g"$) is an exciton and PA_1 gives the lower limit of the exciton binding energy.

ergy of the optical exciton), however, depend primarily[48,58] on the values of U and V_{ij}, which are expected to be nearly the same in the polymers and the S-SWCNTs, and weakly on t_{ij}. We expect calculated energy differences in the S-SWCNTs to be correct at a semiquantitative level, even though current absolute energies are slightly too high.[58] We did not include in Fig. 6 the $m'\,^1A_g$ states that are coupled to the dark excitons, as they will be indistinguishable in their energies from the $m\,^1A_g$ states on this scale. For comparison, we have also included in the figure the excitonic energy spectrum of PPV, calculated within the PPP Hamiltonian of Eq. (2) with the same parameters. Within SCI theory, all states below the H-F thresholds within the same manifold are excitons. For the (10,0) zigzag S-SWCNT we have also shown the higher energy $n\,^1B_u$ state in the $n=1$ manifold. As with the π-conjugated polymers,[28,35,48] this state is identified by its large dipole couplings with the $m\,^1A_g$. Importantly, in both the (10,0) and the (6,2) S-SWCNTs, the $m\,^1A_g$ and $m"\,^1A_g"$ states occur below the respective H-F thresholds, indicating that exactly as in the π-conjugated polymers, the energy locations of these excitonic two-photon states give the lower bound to the exciton binding energy.

In Table II we have summarized the calculated results for all the S-SWCNTs we have studied. We give the calculated PA energies that originate from both the $Ex1$ and the $D1$ excitons, as well as the corresponding H-F thresholds for the $n=1$ manifold. Note that for S-SWCNTs with diameters 0.8–1.3 nm, the calculated range of PA energies, about 0.25–0.55 eV, matches closely with the experimental width of the PA_1 band in Fig. 2. As we have already indicated, PA_2 is not due to excited state absorption from the $n=1$ excitons to states in the higher manifold, and this indicates that the most likely origin of PA_2 is the same as that in PPV. In Fig. 2 we have indicated that the continuum band threshold in PPV and PFO lies in between PA_1 and PA_2, in view of both theoretical and experimental work. Based on the overall experimental similarities that we find between the π-conjugated polymers and S-SWCNTs, and the theoretical

TABLE II. Summary of computed results for different S-SWCNTs. Here $E^{Ex1}_{PA_1}$ and $E^{D1}_{PA_1}$ are PA_1 energies that correspond to excited state absorptions from the $Ex1$ and $D1$, respectively. E_{b1} is the binding energy of $Ex1$, as measured by the energy difference between the H-F band threshold and the energy of $Ex1$.

NT	d (Å)	$E^{Ex1}_{PA_1}$ (eV)	$E^{D1}_{PA_1}$ (eV)	E_{b1} (eV)
(7,0)	5.56	0.42	0.54	0.54
(6,2)	5.72	0.41–0.44	0.47	0.52
(8,0)	6.35	0.37	0.47	0.53
(6,4)	6.92	0.36	0.41	0.48
(10,0)	7.94	0.36	0.49	0.41
(11,0)	8.73	0.31	0.40	0.41
(7,6)	8.95	0.28–0.33	0.38	0.39
(13,0)	10.3	0.31	0.43	0.32
(14,0)	11.1	0.28	0.37	0.34
(17,0)	13.5	0.27	0.35	0.29

energy spectra, it is then natural to guess that the location of the $n=1$ continuum band threshold in S-SWCNTs also lies between the peaks of the PA_1 and PA_2 absorption bands. This would give lowest exciton binding energies of about 0.3 eV in the widest S-SWCNTs, in excellent agreement with the calculations.

V. DISCUSSIONS AND CONCLUSIONS

Our principal conclusion is that the energy spectrum within the $n=1$ energy manifold of S-SWCNTs is very similar to the energy spectrum of π-conjugated polymers. Aside from modifications due to the existence of the dark excitons in the S-SWCNTs and $m"\,^1A_g"$ bands in the chiral S-SWCNTs, the same essential states model of third order optical nonlinearity applies to both systems. The origin of the low energy PA_1 in both S-SWCNTs and π-conjugated polymers is then excited state absorption from $Ex1$ and $D1$ to higher energy two-photon excitons. The broad nature of the PA_1 band in the S-SWCNTs arises from the inhomogeneous nature of the experimental sample, with SWCNT bundles that contain a distribution of S-SWCNTs with different diameters and exciton binding energies. If we assume that the peak in the PA_1 band corresponds to those S-SWCNTs that dominate nonlinear absorption, then the low energy of the peak in the PA_1 band in Fig. 2, taken together with the data in Table II, suggest that PA is dominated by the widest S-SWCNTs in our sample. The common origin of PA_1 and PA_2 (see Fig. 3) indicates that PA_2 is also dominated by the widest S-SWCNTs. The peak in the PA_2 band at $\sim$0.7 eV is then due to the widest S-SWCNTs, with PA_2 due to narrower S-SWCNTs occurring at even higher energies. Hence the energy region 0.2–0.55 eV in Fig. 2(c) must correspond only to PA_1 excitations. Based on the similarities in the energy spectra of the S-SWCNTs and the π-conjugated polymers in Fig. 6, we can therefore construct the vertical dashed line in Fig. 2(c), which identifies the threshold of the continuum band for the widest S-SWCNTs in the film. Exciton binding

energies of about 0.3–0.4 eV are then predicted for those S-SWCNTs in the film that dominate the nonlinear absorption. For S-SWCNTs with diameters ~0.8 nm, Wang *et al.* found TPA at energies very close to the peak of our PA_1 band, and based on additional estimates from the 1D hydrogenic exciton theory, determined their exciton binding energies to be also about 0.4 eV.[23] Remarkably, our calculated binding energies of the excitons for S-SWCNTs with diameters in this range are very close in Table II. We believe that this coincidence in the calculated and observed experimental exciton binding energies for the S-SWCNTs is not fortuitous. Within the PPP Hamiltonian the exciton binding energy depends primarily on the long range Coulomb interactions in Eq. (3). The parametrization of Eq. (3) for PPV was arrived at following an extensive search across 15 sets of (U,κ) values in Ref. 32, and only the parameter set $U=8$ eV, $\kappa=2$ reproduced all four linear absorption bands (at 2.4, 3.7, 4.7, and 6 eV, respectively) and the experimentally observed energies of the $m\,^1A_g$ (Refs. 25 and 26) and the $1\,^3B_u$.[56] The successful transferability of the parameters from PPV to S-SWCNTs then suggests that the Coulomb interaction parameters as well as the background dielectric constants in these two classes of materials are close in magnitude. This in turn justifies the use of π-electron models for the S-SWCNTs, at least for the widest S-SWCNTs which dominate the nonlinear absorption. More careful fitting of the one-electron parameter t_{ij}, which requires comparison of the calculated and experimental absolute energies of the optical excitons for a suitably large number of S-SWCNTs, is currently in progress.[58]

The similarity in the photophysics of S-SWCNTs and π-conjugated polymers suggests several directions for future research. Theoretically, determination of the proper mechanism of PA_2 in analogy to the existing results for π-conjugated polymers[51] is a high priority. The energy location of the lowest triplet exciton and triplet PA energy in S-SWCNTs are also of strong experimental and theoretical interest. The energy difference between the lowest singlet and triplet excitons is a measure of the strength of Coulomb interactions, while calculations of triplet PA provide yet another check for the model Hamiltonian of Eq. (2). S-SWCNTs also provide us with a unique opportunity of extending nonlinear spectroscopy to the very interesting region of the $n=2$ energy manifolds. Exciton states in the $n=2$ manifold lie deep inside the $n=1$ continuum band and can be expected to exhibit novel optical behavior. Whether or not the $n=2$ manifold has the same structure as the $n=1$ manifold is an intriguing question. Although neither TPA nor PM experiments can reach the two-photon states in this region, these should become visible in electroabsorption measurements. Theoretical and experimental works along these directions are currently in progress.

ACKNOWLEDGMENTS

We thank Ray H. Baughman and Alan B. Dalton (Nanotech Institute, UT Dallas) for supplying the SWCNT samples. Work at the University of Arizona was supported by NSF-DMR-0406604. Work at the University of Utah was supported by DOE FG-04-ER46109.

[1] A. B. Dalton, S. Collins, E. Muñoz, J. M. Razal, V. H. Ebron, J. P. Ferraris, J. N. Coleman, B. G. Kim, and R. H. Baughman, Nature **423**, 703 (2003).
[2] P. G. Collins, A. Zettl, H. Bando, A. Thess, and R. E. Smalley, Science **278**, 100 (1997).
[3] J. A. Misewich, R. Martel, Ph. Avouris, J. C. Tsang, S. Heinze, and J. Tersoff, Science **300**, 783 (2003).
[4] T. Hertel and G. Moos, Phys. Rev. Lett. **84**, 5002 (2000).
[5] M. J. O'Connell, S. M. Bachilo, C. B. Huffman, V. C. Moore, M. S. Strano, E. H. Haroz, K. L. Rialon, P. J. Boul, W. H. Noon, C. Kittrell, J. Ma, R. H. Hauge, R. B. Weisman, and R. E. Smalley, Science **297**, 593 (2002).
[6] R. Saito, G. Dresselhaus, and M. S. Dresselhaus, *Physical Properties of Carbon Nanotubes* (Imperial College Press, London, 1998).
[7] T. Ogawa and T. Takagahara, Phys. Rev. B **44**, 8138 (1991).
[8] T. Ando, J. Phys. Soc. Jpn. **66**, 1066 (1997).
[9] M. F. Lin, Phys. Rev. B **62**, 13153 (2000).
[10] C. L. Kane and E. J. Mele, Phys. Rev. Lett. **90**, 207401 (2003).
[11] C. L. Kane and E. J. Mele, Phys. Rev. Lett. **93**, 197402 (2004).
[12] C. D. Spataru, S. Ismail-Beigi, L. X. Benedict, and S. G. Louie, Phys. Rev. Lett. **92**, 077402 (2004).
[13] R. B. Capaz, C. D. Spataru, P. Tangney, M. L. Cohen, and S. G. Louie, Phys. Rev. Lett. **94**, 036801 (2005).
[14] E. Chang, G. Bussi, A. Ruini, and E. Molinari, Phys. Rev. Lett. **92**, 196401 (2004).
[15] H. Zhao and S. Mazumdar, Phys. Rev. Lett. **93**, 157402 (2004).
[16] V. Perebeinos, J. Tersoff, and Ph. Avouris, Phys. Rev. Lett. **92**, 257402 (2004).
[17] V. Perebeinos, J. Tersoff, and Ph. Avouris, Phys. Rev. Lett. **94**, 027402 (2005).
[18] J.-S. Lauret, C. Voisin, G. Cassabois, C. Delalande, P. Roussignol, O. Jost, and L. Capes, Phys. Rev. Lett. **90**, 057404 (2003).
[19] O. J. Korovyanko, C.-X. Sheng, Z. V. Vardeny, A. B. Dalton, and R. H. Baughman, Phys. Rev. Lett. **92**, 017403 (2004).
[20] Y.-Z. Ma, J. Stenger, J. Zimmermann, S. M. Bachilo, R. E. Smalley, R. B. Weisman, and G. R. Fleming, J. Chem. Phys. **120**, 3368 (2004).
[21] C.-X. Sheng, Z. V. Vardeny, A. B. Dalton, and R. H. Baughman, Phys. Rev. B **71**, 125427 (2005).
[22] C. Manzoni, A. Gambetta, E. Menna, M. Meneghetti, G. Lanzani, and G. Cerullo, Phys. Rev. Lett. **94**, 207401 (2005).
[23] F. Wang, G. Dukovic, L. E. Brus, and T. F. Heinz, Science **308**, 838 (2005).
[24] J. W. Kennedy, Z. V. Vardeny, S. Collins, R. H. Baughman, H. Zhao, and S. Mazumdar, cond-mat/0505071 (unpublished).
[25] S. V. Frolov, Z. Bao, M. Wohlgenannt, and Z. V. Vardeny, Phys. Rev. Lett. **85**, 2196 (2000).
[26] S. V. Frolov, C. Kloc, B. Batlogg, M. Wohlgenannt, X. Jiang, and Z. V. Vardeny, Phys. Rev. B **63**, 205203 (2001).

[27] S. N. Dixit, D. Guo, and S. Mazumdar, Phys. Rev. B **43**, 6781 (1991).
[28] D. Guo, S. Mazumdar, S. N. Dixit, F. Kajzar, F. Jarka, Y. Kawabe, and N. Peyghambarian, Phys. Rev. B **48**, 1433 (1993).
[29] P. C. M. McWilliams, G. W. Hayden, and Z. G. Soos, Phys. Rev. B **43**, 9777 (1991).
[30] S. Abe, M. Schreiber, W. P. Su, and J. Yu, Phys. Rev. B **45**, 9432 (1992).
[31] D. Beljonne, J. Cornil, Z. Shuai, J. L. Brédas, F. Rohlfing, D. D. C. Bradley, W. E. Torruellas, V. Ricci, and G. I. Stegeman, Phys. Rev. B **55**, 1505 (1997).
[32] M. Chandross, S. Mazumdar, M. Liess, P. A. Lane, Z. V. Vardeny, M. Hamaguchi, and K. Yoshino, Phys. Rev. B **55**, 1486 (1997); M. Chandross and S. Mazumdar, *ibid.* **55**, 1497 (1997).
[33] S. Ramasesha, S. K. Pati, Z. Shuai, and J. L. Brédas, Adv. Quantum Chem. **38**, 121 (2000).
[34] M. Yu. Lavrentiev, W. Barford, S. J. Martin, H. Daly, and R. J. Bursill, Phys. Rev. B **59**, 9987 (1999).
[35] A. Race, W. Barford, and R. J. Bursill, Phys. Rev. B **64**, 035208 (2001).
[36] M. Hamaguchi and K. Yoshino, Jpn. J. Appl. Phys., Part 2 **33**, L1478 (1994).
[37] M. Kasha, Discuss. Faraday Soc. **9**, 14 (1950).
[38] A. J. Cadby, P. A. Lane, H. Mellor, S. J. Martin, M. Grell, C. Giebeler, D. D. C. Bradley, M. Wohlgenannt, C. An, and Z. V. Vardeny, Phys. Rev. B **62**, 15604 (2000).
[39] R. Hidayat, S. Tatsuhara, D. W. Kim, M. Ozaki, K. Yoshino, M. Teraguchi, and T. Masuda, Phys. Rev. B **61**, 10167 (2000).
[40] F. Wang, G. Dukovic, L. E. Brus, and T. F. Heinz, Phys. Rev. Lett. **92**, 177401 (2004).
[41] H. Htoon, M. J. O'Connell, S. K. Doorn, and V. I. Klimov, Phys. Rev. Lett. **94**, 127403 (2005).
[42] J. I. Pankove, *Optical Processes in Semiconductors* (Prentice-Hall, Englewood Cliffs, NJ, 1971).
[43] S. Reich, M. Dworzak, A. Hoffmann, C. Thomsen, and M. S. Strano, Phys. Rev. B **71**, 033402 (2005).
[44] V. Perebeinos, J. Tersoff, and Ph. Avouris, cond-mat/0506775 (unpublished).
[45] C. D. Spataru, S. Ismail-Beigi, R. B. Capaz, and S. G. Louie, Phys. Rev. Lett. **95**, 247402 (2005).
[46] R. Pariser and R. G. Parr, J. Chem. Phys. **21**, 466 (1953); **21**, 767 (1953).
[47] J. A. Pople, Trans. Faraday Soc. **49**, 1375 (1953).
[48] M. Chandross, Y. Shimoi, and S. Mazumdar, Phys. Rev. B **59**, 4822 (1999).
[49] B. Lawrence, W. E. Torruellas, M. Cha, M. L. Sundheimer, G. I. Stegeman, J. Meth, S. Etemad, and G. Baker, Phys. Rev. Lett. **73**, 597 (1994).
[50] M. Liess, S. Jeglinski, Z. V. Vardeny, M. Ozaki, K. Yoshino, Y. Ding, and T. Barton, Phys. Rev. B **56**, 15712 (1997).
[51] A. Shukla, H. Ghosh, and S. Mazumdar, Phys. Rev. B **67**, 245203 (2003).
[52] J. A. Pople, Proc. Phys. Soc., London, Sect. A **68**, 81 (1955).
[53] S. Mazumdar, F. Guo, K. Meissner, B. Fluegel, N. Peyghgambarian, M. Kuwata-Gonokami, Y. Sato, K. Ema, R. Shimano, T. Tokihiro, H. Ezaki, and E. Hanamura, J. Chem. Phys. **104**, 9283 (1996).
[54] L. Salem, *The Molecular Orbital Theory of Conjugated Systems* (W. A. Benjamin, Inc., New York, 1966). See also, D. Baeriswyl, D. K. Campbell, and S. Mazumdar, in *Conjugated Conducting Polymers*, edited by H. Kiess (Springer-Verlag, Berlin, 1992), and W. Barford, *Electronic and Optical Properties of Conjugated Polymers* (Oxford University Press, Oxford, 2005).
[55] K. Ohno, Theor. Chim. Acta **2**, 219 (1964).
[56] A. P. Monkman, H. D. Burrows, L. J. Hartwell, L. E. Horsburgh, I. Hamblett, and S. Navaratnam, Phys. Rev. Lett. **86**, 1358 (2001).
[57] C. W. M. Castleton and W. Barford, J. Chem. Phys. **117**, 3570 (2002).
[58] Z. Wang, H. Zhao, and S. Mazumdar (unpublished).